Journal of the Korean Physical Society, Vol. 69, No. 3, August 2016, pp. 390∼397

Prominent Ethanol Sensing with Cr_2O_3 Nanoparticle-Decorated ZnS Nanorods Sensors

Gun-Joo Sun, Hyejoon Kheel, Tae-Gyung Ko and Chongmu Lee*
Department of Materials Science and Engineering, Inha University, Incheon 22212, Korea

Hyoun Woo Kim
Department of Materials Science and Engineering, Hanyang University, Seoul 04763, Korea

(Received 28 December 2015)

ZnS nanorods and Cr_2O_3 nanoparticle-decorated ZnS nanorods were synthesized by using facile hydrothermal techniques, and their ethanol sensing properties were examined. X-ray diffraction and scanning electron microscopy revealed good crystallinity and size uniformity for the ZnS nanorods. The Cr_2O_3 nanoparticle-decorated ZnS nanorod sensor showed a stronger response to ethanol than the pristine ZnS nanorod sensor. The responses of the pristine and the decorated nanorod sensors to 200 ppm of ethanol at 300 °C were 2.9 and 13.8, respectively. Furthermore, under these conditions, the decorated nanorod sensor showed a longer response time (23 s) and a shorter recovery time (20 s) than the pristine one did (19 and 35 s, respectively). Consequently, the total sensing time of the decorated nanorod sensor (42 s) was shorter than that of the pristine one (55 s). The decorated nanorod sensor showed excellent selectivity to ethanol over other volatile organic compound gases including acetone, methanol, benzene, and toluene whereas the pristine one failed to show selectivity to ethanol over acetone. The improved sensing performance of the decorated nanorod sensor is attributed to a modulation of the width of the conduction channel and the height of the potential barrier at the ZnS-Cr_2O_3 interface accompanying the adsorption and the desorption of ethanol gas, and the greater surface-to-volume ratio of the decorated nanorods which was greater than that of the pristine one due to the existence of the ZnS-Cr_2O_3 interface.

PACS numbers: 81.07.-b, 81.05.Ea, 81.15.Gh, 85.35.-p
Keywords: Hydrothermal, ZnS, Cr_2O_3, Gas sensor, Ethanol
DOI: 10.3938/jkps.69.390

I. INTRODUCTION

The remarkable fundamental properties of zinc sulfide (ZnS) has allowed it to have diverse applications such as light-emitting diodes, lasers, flat panel displays, infrared windows, sensors, biodevices, *etc.* [1]. In particular, ZnS can be applied to the fabrication of ultraviolet (UV) light sensors and gas sensors. Over the past decade, the following ZnS nanostructure-based gas sensors have been reported: a ZnS single nanobelt sensor for H_2 sensing [1], ZnS nanobelt sensors for H_2 sensing [2], and ZnS microsphere sensors for O_2 sensing [3], ZnS nanowire sensors for acetone and ethanol sensing [4], ZnS nanotube array sensors for humidity sensing [5]. However, reports on ZnS nanostructures-based gas sensors are very few compared to those on meta-oxide semiconductor nanostructures-based gas sensors [1–5].

Metal-oxide semiconductors are endowed with many good properties, such as high sensitivity, fast sensing, low detection limits and function durability, that sensor materials should have. On the other hand, this sensing material, a metal-oxide semiconductor, has several shortcomings such as high operation temperature, poor selectivity and reliability. A range of techniques, including doping, heterostructure formation and light activation, have been studied to overcome these drawbacks. Of these techniques, the heterostructure formation technique was adopted in this study to overcome the poor performance of the SnO_2 1D nanostructure-based sensors. The formation of heterostructures by creating interfaces between two dissimilar semiconducting materials can cause the Fermi levels across the interface to be equal, *i.e.*, in equilibrium, resulting in charge transfer and the formation of an interfacial depletion region. This will eventually lead to enhanced sensor performance. The enhanced sensing properties of these heterostructures might be attributed to many factors, including electronic effects such as band bending due to Fermi level equilibration, charge carrier separation, depletion layer manipulation and increased interfacial potential barrier energy; chemical effects such

*E-mail: cmlee@inha.ac.kr; Fax: +82-32-862-5546

as decrease in the activation energy, targeted catalytic activity and synergistic surface reactions; and geometrical effects such as grain refinement, surface area enhancement, and increased gas accessibility [6]. Heterostructure formation is commonly achieved by either forming core-shell structures by coating nanostructures with a thin film or decorating nanostructures with dissimilar semiconductor nanoparticles. In this paper, we report the synthesis of Cr_2O_3 nanoparticle-decorated ZnS nanorods via a facile hydrothermal route and their enhanced sensing properties for ethanol (C_2H_5OH) gas.

II. EXPERIMENTAL PROCEDURE

1. Synthesis of Pristine and Cr_2O_3 Nanoparticle-Decorated ZnS Nanorods

The Cr_2O_3 nanoparticle-decorated ZnS nanorods were synthesized via a facile hydrothermal route: ZnS nanorods were synthesized by using a hydrothermal method. First, Au-coated sapphire was used as a substrate for the synthesis of the ZnS nanorods. Au was deposited on a silicon (100) substrate by direct current (dc) magnetron sputtering. A quartz tube was mounted horizontally inside a tube furnace. An alumina boat containing 99.99% pure ZnS powders and the silicon substrates were placed separately in a two-heating zone-tube furnace, where the ZnS powders were in the first heating zone and the Si substrates in the second heating zone. The substrate temperatures of the first and the second heating zones were set to 850 and 650 °C, respectively, with an ambient nitrogen gas pressure and a flow rate of 1 Torr and 50 cm^3/min, respectively, throughout the synthesis process. The thermal evaporation process was carried out for 1 h; then, the furnace was cooled to room temperature at 1 mTorr, after which the products were taken out.

Next, 50-mM Cr_2O_3 precursor solution was prepared by dissolving chromium acetate monohydrate ($Cr(CH_3COO)_2{\cdot}H_2O$) in distilled water. Fifty ml of the Cr_2O_3 precursor solution and 10 ml of 28% NH_4OH solution were mixed together. The mixed solution was ultrasonicated for 30 min to form a uniform solution and then rotated using a centrifuge at 5,000 rpm for 2 min to precipitate the Cr_2O_3 powders. The precipitated powders were collected by removing the liquid and leaving the powders behind. The collected powders were rinsed in a 1:1 solution of isopropyl alcohol (IPA) and distilled water to remove the impurities. The rinsing process was repeated five times. Subsequently, the Cr_2O_3 precursor solution was dropped onto the ZnS nanorods on a substrate, and the substrate was rotated at 1,000 rpm for 30 s for Cr_2O_3 decoration. After the spin-coating process, the Cr_2O_3-decorated ZnS nanorod sample was dried at 150 °C for 1 min and then annealed in air at 500 °C for 1 h.

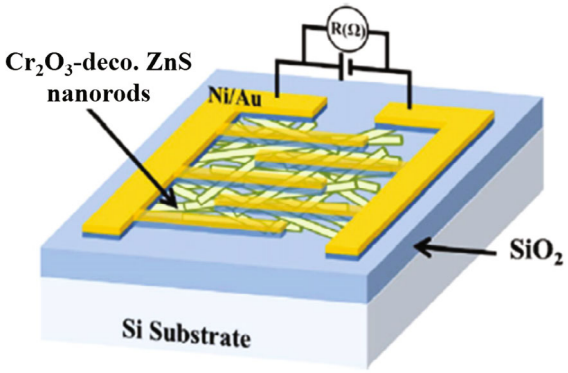

Fig. 1. (Color online) Schematic of the sensor's structure.

2. Materials Characterizations of the Materials

The phase and the crystallinity of the pristine and the Cr_2O_3 nanoparticle-decorated ZnS nanorods were analyzed by using XRD (Philips X′pert MRD) with Cu Kα radiation (1.5406 Å). The data were collected over the 2θ range $20 - 80°$ with a step size of $0.05°$ 2θ at a scan speed of 0.05 °/s. Assignment of the XRD peaks and identification of the crystalline phases were carried out by comparing the obtained data with the reference compounds in the JCPDS database. The morphology and the particle size of the synthesized powders were examined by using scanning electron microscopy (SEM, Hitachi S-4200) at an accelerating voltage of 5 kV.

3. Sensor Fabrication

For the sensing measurement, a SiO_2 film (∼200 nm) was grown thermally on single-crystalline Si (100). Then, the as-synthesized ZnS nanorods and Cr_2O_3 nanoparticle-decorated ZnS nanorods were dispersed in a 1:1 mixture of deionized water and isopropyl alcohol by ultrasonication. The Cr_2O_3 nanoparticle-decorated ZnS nanorod sensors were fabricated by pouring a few drops of ethanol with suspended nanorods onto the SiO_2-coated Si substrates equipped with a pair of interdigitated electrodes (IDE), Ni (∼10 nm)/Au (∼100 nm) with a 20 μm gap (Fig. 1).

4. Sensing Tests

The electrical and the gas sensing properties of the pristine and Cr_2O_3 nanoparticle-decorated ZnS nanorods in a quartz tube inserted in an electrical furnace were determined at different temperatures. During the tests, the nanorod gas sensors were placed in a sealed quartz tube with an electrical feed through. A predetermined amount of ethanol (> 99.99%) gas was injected into the

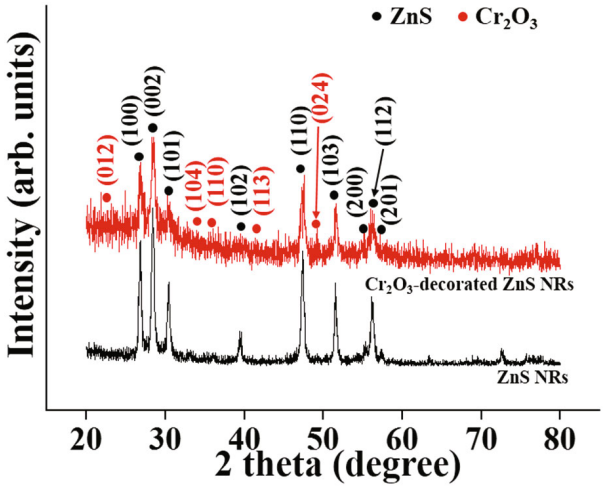

Fig. 2. (Color online) XRD patterns of the pristine and the Cr_2O_3 nanoparticle-decorated ZnS nanorods

testing tube through a microsyringe to obtain ethanol concentrations of 10, 20, 50, 100, and 200 ppm while the electrical resistance of the nanorods was monitored. The response was defined as R_g/R_a, where R_g and R_a are the electrical resistances of sensors in ethanol gas and air, respectively. The response time was defined as the time needed for the change in the electrical resistance to reach 90% of the equilibrium value after the ethanol had been injected, and the recovery time was defined as the time needed for the sensor to return to 90% of the original resistance in air after the ethanol gas had been removed.

III. RESULTS AND DISCUSSION

1. Crystalline Structure and Morphology

The structure and the chemical composition of pristine and Cr_2O_3 nanoparticle-decorated ZnS nanorods were examined immediately after sample preparation byusing XRD. As shown in Fig. 2, all the XRD peaks marked by the red circles were consistent with the standard value of the Cr_2O_3 phase (JCPDS No. 84-1616). The peaks marked by the black circles were attributed to the formation of the ZnS phase (JCPDS No. 89-2942). The fact that no distinct peaks existed, except those of Cr_2O_3 and ZnS, indicates that no other phases had formed, highlighting the purity of the final products. The (200) plane was chosen to calculate the crystallite size of the pristine and the Cr_2O_3 nanoparticle-decorated ZnS nanorods by using the Scherrer formula [7].

$$D = K\lambda/\beta\cos\theta, \quad (1)$$

where D is the crystallite size in nm, K is the shape factor (0.90), λ is the wavelength of X-rays used (1.5406 Å), β is the fullwidth at half maximum in degrees and θ is the diffraction angle in degrees. The values obtained were 60 nm and 50 nm for the pristine and the Cr_2O_3 nanoparticle-decorated ZnS nanorods, respectively.

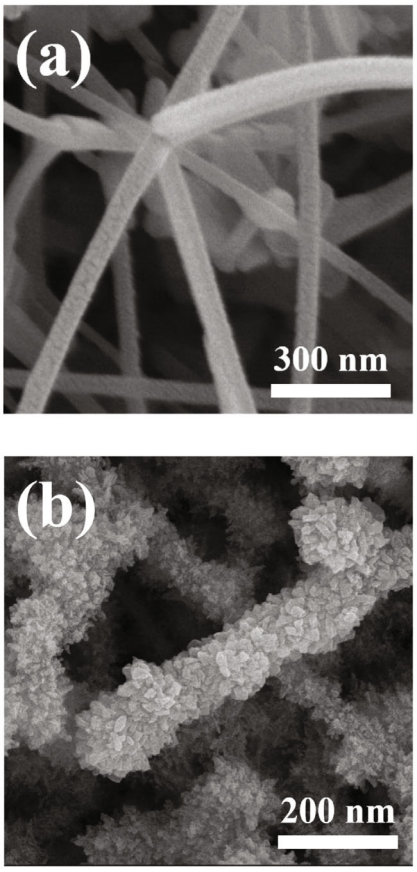

Fig. 3. SEM images (a) the pristine ZnS nanorods and (b) the Cr_2O_3 nanoparticle-decorated ZnS nanorods.

Figures 3(a) and (b) show SEM images of pristine and Cr_2O_3 nanoparticle-decorated ZnS nanorods, respectively. The pristine ZnS nanorods were $50 - 100$ nm in diameter and up to a few tens of micrometers in length. The entire surfaces of the ZnS nanorods in the decorated nanorods are completely covered with many lenticular-shaped Cr_2O_3 nanoparticles with long radii of $30 - 40$ nm and small radii of $10 - 20$ nm (Fig. 3(b)). The surface-to-volume ratio of the decorated nanorods must be much higher than that of the pristine nanorods.

2. Gas-Sensing Properties

A. Optimal Working Temperature

The sensitivity of gas sensors is strongly influenced by the operating temperature. Parallel experiments were carried out over the temperature range from 200 to 400 °C to determine the optimal operating temperature of

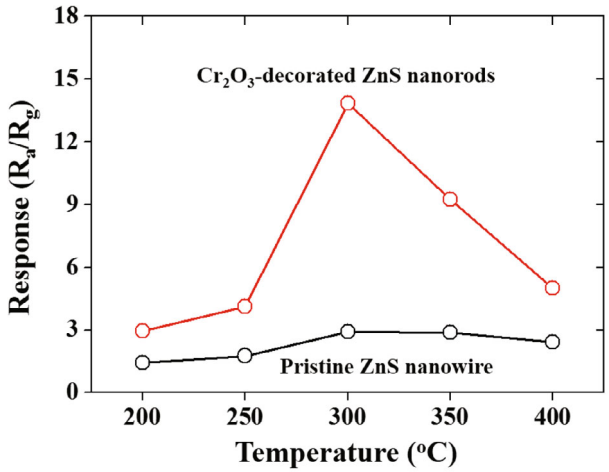

Fig. 4. (Color online) Responses of the pristine and the Cr_2O_3 nanoparticle-decorated ZnS sensors to 200 ppm of ethanol at different temperatures.

the sensors. Figure 4 shows the relationship between the response of the pristine and the Cr_2O_3 nanoparticle-decorated ZnS nanorod sensors to 200 ppm of ethanol in the temperature range of 200 − 400 °C. Both the pristine and the Cr_2O_3 nanoparticle-decorated ZnS nanorod sensors showed a maximum response at 300 °C, suggesting that 300 °C is the optimal operating temperature for both sensors.

The temperature dependence of the sensor response is generally controlled by two parameters: the reaction rate between the adsorbed oxygen ions and ethanol molecules, and the electron density of the sensor. The reaction rate coefficient and the electron density increase exponentially with increasing temperature. On the other hand, the sensor response is proportional to the reaction rate coefficient and inversely proportional to the electron density. These two parameters compete with each other and result in a maximum sensor response at the optimal operating temperature [8].

B. Sensor Response for various Ethanol Gas Concentration

Figures 5(a) and (b) present the gas response transients of the pristine and the Cr_2O_3 nanoparticle-decorated ZnS nanorod sensors, respectively, for 5, 10, 50, 100, and 200 ppm of ethanol gas at 300 °C. For both sensors, the response was fully reversible and both sensors exhibited n-type behavior upon exposure to ethanol gas.

Figure 6 shows the calibration curves for the responses of the two sensors to different ethanol concentrations, and clearly shows that the response of the Cr_2O_3 nanoparticle-decorated ZnS nanorod sensor to every ethanol concentration was stronger than that of the

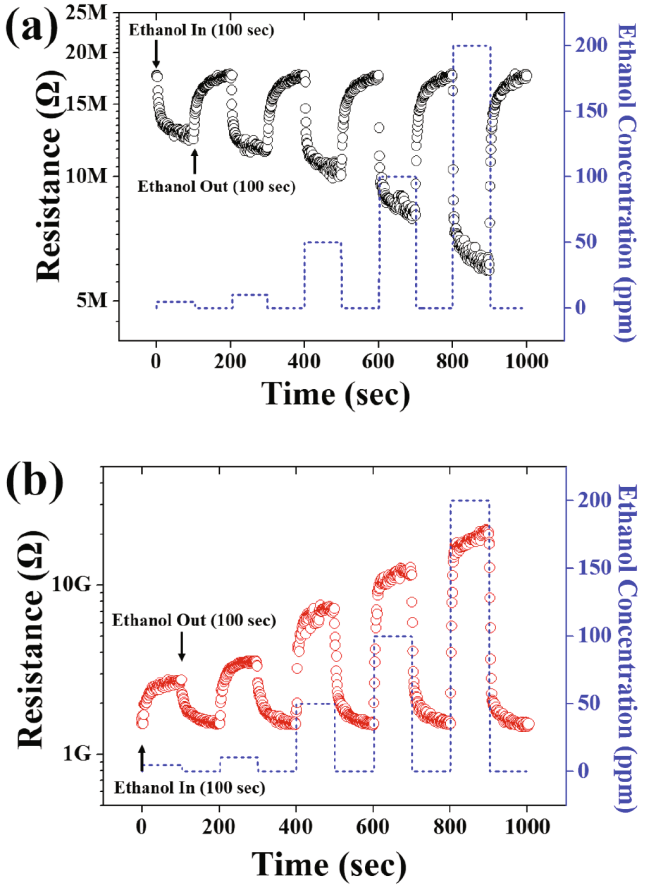

Fig. 5. (Color online) Gas response transients of (a) the pristine ZnS nanorod sensors and (b) the Cr_2O_3 nanoparticle-decorated ZnS nanorod sensors for 5, 10, 50, 100, and 200 ppm of ethanol gas at 300 °C.

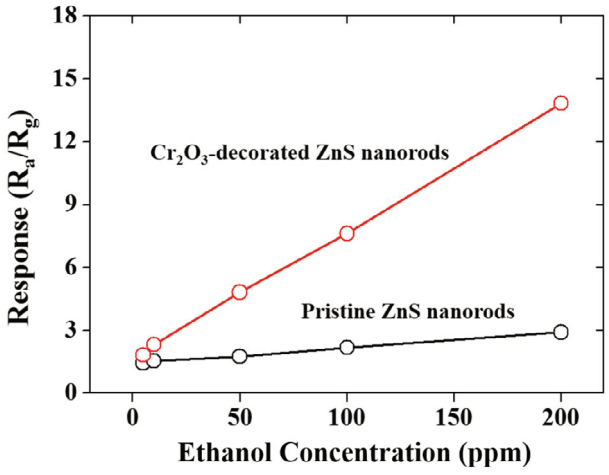

Fig. 6. (Color online) Responses of the pristine and the Cr_2O_3 nanoparticle-decorated ZnS nanorod sensors to different ethanol concentrations at 300 °C.

pristine one. As an example, the response of the Cr_2O_3 nanoparticle-decorated ZnS nanorod sensor to 200 ppm

of ethanol was approximately 4.5 times stronger than that of the pristine one. The Occupational Safety Health Administration (OSHA) established the maximum recommended exposure level of ethanol to be 1000 ppm [9], and the Cr_2O_3 nanoparticle-decorated ZnS nanorod sensor will easily be able to detect this level of ethanol.

A relationship between the sensor response ($S = R_g/R_a$) and the ethanol concentration can be expressed as an empirical equation:

$$S = R_g/R_a = A[C_{ethanol}]^b + 1, \quad (2)$$

where A, b and $[C_{ethanol}]$ are a constant, an exponent and the ethanol concentration, respectively [10]. In fact, "b" is a charge parameter with an ideal value of 1 for O^- and 0.5 for O^{2-}, which is derived from the surface interaction between chemisorbed oxygen and the target gas [11,12]. The response of the decorated nanorod sensor tended to increase more rapidly than that of the pristine one as the ethanol concentration was increased, suggesting that the response of the former to ethanol would be much stronger than that of the latter at high ethanol concentrations.

C. Response and Recovery Times

Figures 7(a) and (b) present the response and the recovery times of the two sensors for 200 ppm of ethanol at 300 °C, respectively. As shown in Figs. 7(a) and (b), the response and recovery times of the two sensors became shorter with increasing ethanol concentration. The change in response time can be explained by a change in the saturation time and by the mean residence period of the ethanol molecules on the sensor's surface. When the ethanol concentration is low, it spends a relatively long time reacting with adsorbed oxygen species. With increasing ethanol concentration, more ethanol molecules are available for the reaction with adsorbed oxygen, resulting in a decrease in response time. The change in recovery time with ethanol concentration can be explained by the structure of the sensors and the diffusion rate. When air is injected into the test chamber, oxygen molecules will diffuse to the surface of the sensors to react with the ethanol molecules. A complete desorption reaction on the inner surface takes more time than that on the outer surface, leading to a longer recovery time at higher ethanol concentrations, where ethanol is present near the inner surfaces of the sensors.

In the case of the response time, for all ethanol concentrations, the Cr_2O_3 nanoparticle-decorated ZnS nanorod sensor had a slightly longer response time, which is probably due to the far higher resistance of the Cr_2O_3 nanoparticle-decorated ZnS nanorod sensor at 300 °C (Fig. 5(b)). This means that less of the adsorbed oxygen species is on the surface of the decorated nanorod sensor. Therefore, after the ethanol gas is injected, it reacts quite slowly with the adsorbed oxygen species, leading to a longer response time. The shorter recovery time of the Cr_2O_3 nanoparticle-decorated ZnS nanorod sensor is probably due to the faster desorption of ethanol gas because of the lower potential barrier to ethanol desorption in the particular structure of the Cr_2O_3 nanoparticle-decorated ZnS nanorod.

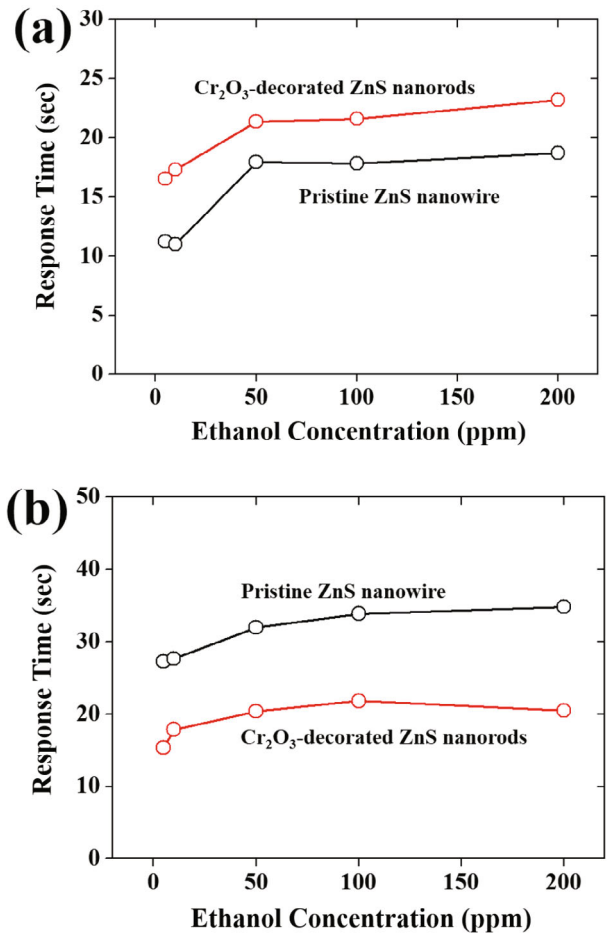

Fig. 7. (Color online) (a) Response times and (b) recovery times of the pristine and the Cr_2O_3 nanoparticle-decorated ZnS nanorod sensors for different ethanol concentrations at 300 °C.

Figure 8 shows that the responses of the pristine and the Cr_2O_3 nanoparticle-decorated ZnS nanorod sensors to ethanol gas at 300 °C were stronger than those to the other volatile organic compound (VOC) gases, indicating that both sensors had excellent selectivity towards ethanol gas. The reason why these ZnS-based sensors have selectivity to ethanol at 300 °C over other gases is not fully understood. The selectivity might be related to the different optimal operating temperatures of the sensors for different target gases. The response of a sensor would depend strongly on the type of gas at different temperatures because different gases have different activation energies for adsorption, desorption and reaction on the semiconductor's surface [13]. For these ZnS-based sensors, 300 °C may be an optimal operating tempera-

Table 1. Comparison of the response, response time and recovery time of the Cr_2O_3 nanoparticle-decorated ZnS nanorod sensor with those of other material 1D nanostructure sensors reported previously.

Nanomaterials	Ethanol conc. (ppm)	Temp. (°C)	Response (%)	Response Time (sec)	Recovery Time (sec)	Ref.
ZnS/ nanorods	200	300	290	19	35	Present work
ZnS/Cr_2O_3 nanorods	200	300	1,384	23	20	Present work
TiO_2 nanotubes	5,000	200	16	-	-	14
SnO_2 nanorods	300	300	3,140	1	1	15
Ce-SnO_2 nanopowders	200	250 − 450	18,500	-	-	16
Pt-SnO_2 nanopowders	100	150 − 350	4,000	12	360	17
SnO_2-ZnO(0.05) composite nanopowders	300	200 − 400	390,000	96 − 418	400 − 600	18
ZnO-SnO_2(0.05) composite nanopowders	300	200 − 400	120,000	96 − 418	400 − 600	18
ZnO nanowires	1,500	300	61	-	-	19
TiO_2 nanobelts	500	250	3,366	1 − 2	1 − 2	20
Ag-TiO_2 nanobelts	500	200	4,171	1 − 2	1 − 2	20
$CoFe_2O_4$ nanopowders	50	150	7190	50	60	21
Co-ZnO nanorods	50	350	987	-	-	22
In_2O_3 nanowires	100	370	200	10	20	23
In_2O_3 nanorods	50	-	795	5	10	24

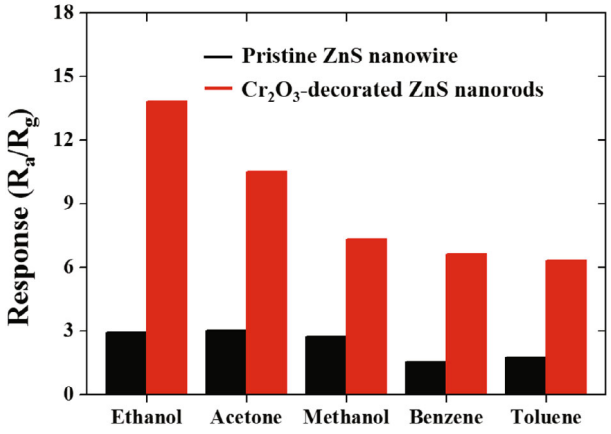

Fig. 8. (Color online) Responses of the pristine and the Cr_2O_3 nanoparticle-decorated ZnS nanorod sensors to different VOC gases.

ture because the activation energy for the adsorption of ethanol is low at that temperature whereas those for the adsorptions of other gas species are relatively high at that temperature.

Up to now, metal-oxide sensors for ethanol detection have been studied extensively. This is because ethanol is used widely in different industries, and its detection in drunk drivers is important for the safetyof society. Table 1 compares the ethano-sensing properties of the pristine and the Cr_2O_3 nanoparticle-decorated ZnS nanorod sensors fabricated in this study with those of other 1D gas sensors reported in the literature [14–24]. The table shows that the response and the response/recovery times of the Cr_2O_3 nanoparticle-decorated ZnS nanorod sensor are comparable to those of metal-oxide semiconductor 1D nanostructured sensors.

D. Gas-Sensing Mechanism

Based on the above results, the Cr_2O_3 nanoparticle-decorated ZnS nanorod sensor showed a significantly improved sensing performance compared to the pristine ZnS sensor. For the pristine ZnS sensor, the gas-sensing mechanism can be explained mainly in terms of the modulation of the depletion layer accompanying the adsorption and the desorption of gases. When the pristine ZnS sensor is exposed to air, oxygen molecules are adsorbed on the surfaces of the ZnS nanorods and are ionized to either O^- or O^{2-} by capturing free electrons from the conduction band of ZnS. This reduces the electron concentration, which then leads to the formation of an electron depletion layer. When ZnS is exposed to ethanol gas, the ethanol molecules react with the oxygen species (O^-, O^{2-}) adsorbed on the surfaces of the ZnS nanorods according to the following equations [25]:

$$C_2H_5OH(\text{gas}) \rightarrow C_2H_5OH(\text{ads}), \quad (3)$$

$$C_2H_5OH(\text{ads}) + 6O^-(\text{ads}) \rightarrow 2CO_2(\text{gas}) + 3H_2O(\text{gas}) + 6e^- \quad (4)$$

These reactions release the trapped electrons back to the conduction band of ZnS, which increases the free electron concentration and ultimately decreases the resistance of the pristine ZnS sensor.

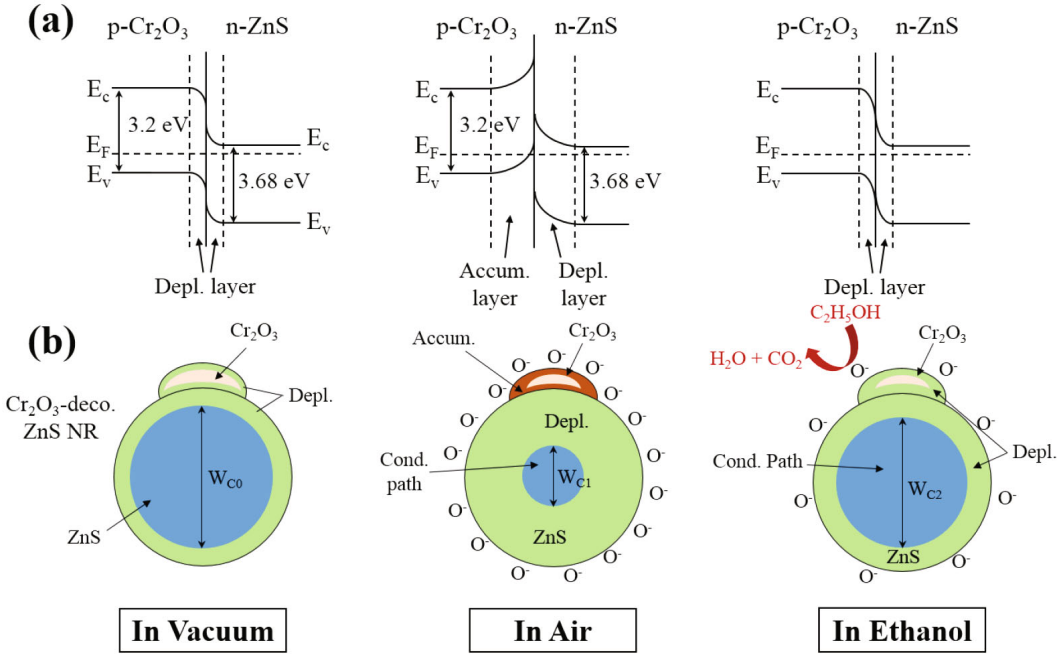

Fig. 9. (Color online) (a) Energy band diagrams of the ZnS-Cr_2O_3 system before and after contact in vacuum, air, and ethanol. (b) Schematics of a cross section of the decorated nanorod and energy band diagram of ZnS-Cr_2O_3 system showing the depletion layer's width and the potential barrier's height in vacuum, air, and ethanol.

On the other hand, for Cr_2O_3 nanoparticle-decorated ZnS nanorod sensor, ZnS and Cr_2O_3 are n-type and p-type semiconductors, respectively, with different electron affinities (3.8 eV for ZnS [26], no data available for Cr_2O_3). Little is known about the electron affinity of Cr_2O_3, but the Fermi energy level of ZnS might be lower than that of Cr_2O_3 because ZnS and Cr_2O_3 are n- and p-type semiconductors, respectively, and the Fermi energy level of a n-type semiconductor is commonly higher than that of a p-type semiconductor. Therefore, the transfer of electrons will occur from the conduction band of Cr_2O_3 to that of ZnS, resulting in two equal Fermi energy levels (E_F) (Fig. 9(a)). This will result in the formation of an electron depletion layer and a potential barrier at the ZnS-Cr_2O_3 n-p junction interface, which will enhance the response of the Cr_2O_3 nanoparticle-decorated ZnS nanorod sensor further compared to that of the pristine one.

The enhanced ethanol-gas-sensing performance of the Cr_2O_3 nanoparticle-decorated ZnS nanorod sensor can be explained by modulation of the conduction channel's width [50] and the potential barrier's height at the ZnS-Cr_2O_3 interface [27, 28]. Figure 9 presents schematic diagrams showing the depletion layer and the potential barrier formed at the ZnS-Cr_2O_3 interface, as well as the energy band diagrams of the ZnS-Cr_2O_3 binary system in air and ethanol gas. The width of the depletion layers formed near the ZnS-Cr_2O_3 interfaces in the Cr_2O_3 nanoparticle-decorated ZnS nanorods is larger than that formed in the surface regions of the pristine ZnS nanorods: (λ_D (ZnS) + λ_D (Cr_2O_3) for the decorated nanorods and λ_D (ZnS_2) for the pristine ZnS nanorods, where λ_D is the Debye length. λ_D (ZnS) = 10^{-5} – 10^{-6} cm [29]. Even though the data for λ_D (Cr_2O_3) are not available at present, a large portion of the total volume of each Cr_2O_3 nanoparticle might be depleted of carriers in air. The larger depletion layer width in the decorated nanorods compared to that in the pristine nanorods, leads to a higher resistivity and a larger change in the resistivity. In addition to the increased depletion layer width, the formation of a potential barrier at the ZnS-Cr_2O_3 interface due to electron trapping in the interface states should be considered when explaining the enhanced response of the decorated nanorods to ethanol gas. Upon exposure to ethanol gas, the potential barrier at the ZnS-Cr_2O_3 interface will decrease whereas after the ethanol gas supply is stopped, the potential barrier will increase upon exposure to air (Fig. 9). Hence, modulation of the potential barrier occurs concomitantly with the adsorption and the desorption of gas molecules, which would increase the change in resistance, *i.e.*, the response of the decorated nanorod sensor to ethanol gas.

In addition to the above two effects, the ZnS-Cr_2O_3 interfaces provide additional. preferential adsorption sites and diffusion paths for oxygen and ethanol molecules [30], which might also contribute to the enhanced ethanol gas sensing properties of the decorated nanorod sensor. In other words, the enhanced response of the Cr_2O_3 nanoparticle-decorated ZnS nanorod sensor is partially attributed to the higher surface-to-volume ratio of the decorated nanorods compared to that of the pristine one because, like the outer surfaces of the nanorods, the ZnS-

Cr_2O_3 interfaces also act as preferential adsorption sites.

IV. CONCLUSION

ZnS nanorods and Cr_2O_3 nanoparticle-decorated ZnS nanorods were synthesized by using hydrothermal techniques. The Cr_2O_3 nanoparticle-decorated ZnS nanorod sensor exhibited a significantly stronger response to ethanol than the pristine one. The decorated nanorod sensor showed a lower working temperature than the other oxide semiconductor 1D nanostructured ethanol gas sensors. This was attributed to the larger modulation of the depletion layer's width, the modulation of the potential barrier's height at the ZnS-Cr_2O_3 interfaces in the ZnS nanorods and Cr_2O_3 nanoparticle-decorated ZnS nanorods, and the crystallographic defects formed at the ZnS-Cr_2O_3 interfaces acting as preferential adsorption sites and diffusion paths for gases. Furthermore, the sensors showed excellent selectivity to ethanol. The favorable gas-sensing performance makes Cr_2O_3 nanoparticle-decorated ZnS nanorods particularly attractive as a promising practical sensor material.

ACKNOWLEDGMENTS

This study was supported financially by the 2015 Inha University Research Grant.

REFERENCES

[1] X. Fang, T. Zhai, U. K. Gautam, L. Li, L. Wu, Y. Bando and D. Golberg, Prog. Mater. Sci. **56**, 175 (2011).
[2] Y. G. Liu, P. Feng, X. Y. Xue, S. L. Shi, X. Q. Fu and C. Wang, Appl. Phys. Lett. **90**, 042109 (2007).
[3] L. Yang, J. Han, T. Luo, M. Li, J. Huang, F. Meng and J. Liu, Chem. Asian J. **4**, 174 (2009).
[4] Z. G. Chen, J. Zou, G. Liu, H. F. Lu, F. Li, G. Q. Lu and H. M. Cheng, Nanotechnology **19**, 055710 (2008).
[5] X. Wang, Z. Xie, H. Huang, Z. Liu, D. Chen and G. Shen, J. Mater. Chem. **22**, 6845 (2012).
[6] D. Miller, S. Akbar and P. Morris, Sens. Actuators B **204**, 250 (2014).
[7] S. Liu, M. Xie, Y. Li, X. Guo, W. Ji and W. Ding, Mater. Chem. Phys. **123**, 109 (2010).
[8] N. Hongsith, E. Wongrat, T. Kerdcharoen and S. Choopun, Sens. Actuators B **144**, 67 (2010).
[9] WEB site: (https://www.osha.gov/dts/chemicalsampling/data/CH_239700.html); Ocuupational Safety & Health Administration.
[10] N. Yamazoe, K. Shimanoe, The theory of power laws for semiconductor sensors, Sens. Actuators B **128**, 566 (2008).
[11] V. Modafferi, G. Panzera, A. Donato, P. L. Antnucci, C. Cannilla, N. Donato, D. Spadaro and G. Neri, Sens. Actuators B **163**, 61 (2012).
[12] J. Seo, K. Park, D. Lee, C. Lee, Materials Science and Engineering B **49**, 247 (1997).
[13] N. Kilinç, E. Sennik and Z. Z. Ozuturk, Thin Solid Films **520**, 953 (2011).
[14] Y. J. Chen, X. Y. Xue, Y. G. Wang and T. H. Wang, Appl. Phys. Lett. **87**, 233503 (2005).
[15] F. Pourfayaz, Y. Mortazavi, A. Khodadadi and S. Ajami, Sens. Actuators B **130**, 625 (2008).
[16] G. Neri, A. Bonavita, G. Micali, N. Donato, F. A. Deorsola, P. Mossino, I. Amato and B. De Benedetti, Sens. Actuators B **117**, 196 (2006).
[17] S. Hemmati, A. A. Firooz, A. A. Khodadadi and Y. Mortazavi, Sens. Actuators B **160**, 1298 (2011).
[18] T. J. Hsueh, C. L. Hsu, S. J. Chang and I. C. Chen, Sens. Actuators B **126**, 473 (2007).
[19] C. Lee, H. H. Kim, C. S. Hong, M. N. Kim, S. S. Hong, D. H. Lee and W. I. Lee, J. Mater. Chem. **18**, 4790 (2008).
[20] J. Jun, C. Jin, H. Kim, J. Kang and C. Lee, Appl. Phys. A **96**, 813 (2009).
[21] Y. J. Li, K. M. Li, C. Y. Wang, C. I. Kuo and L. J. Chen, Sens. Actuators B **161**, 734 (2012).
[22] J. T. No, J. H. O and C. Lee, Mater. Chem. Phys. **63**, 44 (2000).
[23] J. Q. Xu, Y. P. Chen, Q. Y. Pan, Q. Xiang, Z. X. Cheng and X. W. Dong, Nanotechnology **18**, 115615 (2007).
[24] Z. Zhu, C. T. Kao and R. J. Wu, Appl. Surf. Sci. **320**, 348 (2014).
[25] B. Sharma and R. Purohit, Semiconductor Hetrojunctions (Pergamon Press, Oxford, 1974).
[26] S. Sung, I. Lim, C. Lee and W. Lee, Chem. Comm. **49**, 6054 (2013).
[27] T. Weis, R. Lipperheide, U. Wille and S. Brehme, J. Appl. Phys. **92**, 1411 (2002).
[28] M. S. Hwang and C. Lee, Mater. Sci. Eng. B **75**, 24 (2000).
[29] L. L. Kazmerski, *Polycrystalline and Amorphous Thin Films and Devices* (Academic Press, San Diego, 1980).
[30] H. Zhang, J. Feng, T. Fei, S. Liu and T. Zhang, Sens. Actuators B **190**, 472 (2014).